Resonant soft x-ray reflectivity of organic thin films

Cheng Wang, Tohru Araki, and Benjamin Watts
Department of Physics, North Carolina State University, Raleigh, North Carolina 27695

Shane Harton
Department of Materials Science and Engineering, North Carolina State University, Raleigh, North Carolina 27695

Tadanori Koga
Chemical and Molecular Engineering Program, Department of Materials Science and Engineering, Stony Brook University, Stony Brook, New York 11794-2275

Saibal Basu
Center of Neutron Research, National Institute of Standard and Technology, Gaithersburg, Maryland 20899

Harald Ade[a)]
Department of Physics, North Carolina State University, Raleigh, North Carolina 27695

(Received 8 December 2006; accepted 26 March 2007; published 23 April 2007)

At photon energies close to absorption edges in the soft x-ray range, the complex index of refraction, $n=1-\delta-i\beta$, of organic materials varies rapidly as a function of photon energy in a manner that strongly depends on the chemical moieties and functionalities present in the material. The authors present details of how these molecular structure specific variations in the complex index of refraction can be utilized to enhance and tune the contrast in reflectivity experiments of organic films. This near edge contrast enhancement mimics the specific contrast achieved through deuterium labeling in neutron reflectivity (NR). This relatively new x-ray approach, resonant soft x-ray reflectivity (RSoXR), thus combines aspects of NR and conventional x-ray reflectivity (XR), yet does not require special chemical procedures. The capabilities of RSoXR are exemplified using a number of polymeric bi- and multilayers. Furthermore, a direct comparison of RSoXR to conventional x-ray reflectivity and NR for polystyrene and poly(methyl methacrylate) bilayers verifies that RSoXR is an excellent alternative tool for the characterization of organic thin films. The influence of the longitudinal and transverse coherence properties as well as the divergence of the x-ray or neutron beam on the capabilities and limitations of each reflectivity variant is discussed.
 [DOI: 10.1116/1.2731352]

I. INTRODUCTION

Currently, a range of experimental characterization techniques with complementary capabilities are widely used to investigate organic surfaces, thin films, and interfaces. These include x-ray photoelectron spectroscopy, secondary ion mass spectrometry, nuclear reaction analysis, forward recoil spectrometry, x-ray reflectivity (XR), and neutron reflectivity (NR).[1–9] Of these, XR and NR are well established research tools for characterizing important parameters of hard- and soft-condensed matter thin films such as film thickness, interfacial width, and interfacial roughness with subnanometer accuracy. In conventional hard x-ray reflectivity, the sensitivity to distinguish materials depends on the electron density, which is typically a strong function of the atomic number Z of the constituent materials. Most organic materials, including natural and synthetic macromolecules, are composed primarily of carbon and hydrogen and a few other, if any, mostly low-Z elements at low concentrations. Differences in electron density in such materials therefore tend to be slight, limiting the observable contrast in conventional XR of organic materials. To improve the analysis capabilities of conventional XR, Seeck *et al.* have developed a Fourier method to analyze low-contrast polymer bilayers.[10] In contrast to x rays, neutrons have highly variable scattering length densities (SLDs) as a function of Z and neutron number N. Since the scattering length of deuterium is 6.671 fm and that of hydrogen is −3.741 fm, high SLD differences and hence high contrast between most organic materials can be achieved by complete or partial deuteration of one of the species. As a complement to XR and NR, Wang *et al.* have recently reported the development of resonant soft x-ray reflectivity (RSoXR) as a thin film characterization method that combines aspects of both NR and XR.[11]

Large changes in reflectivity at an interface and the resulting interference in thin films and multilayers are observed as the complex index of refraction, $n=1-\delta-i\beta$, changes rapidly as a function of photon energy. Tuning the probe beam energy to take advantage of these variations in reflectivity provides RSoXR with "molecular structure specific" sensitivity analogous to deuteration in NR. Through the use of specific energies that typically match extrema or zero crossings in δ or β, the sensitivity to the polymer-polymer or polymer-air interface can be selectively enhanced or suppressed. Yet, no chemical modifications are necessary, a

[a)]Author to whom correspondence should be addressed; electronic mail: harald_ade@ncsu.edu

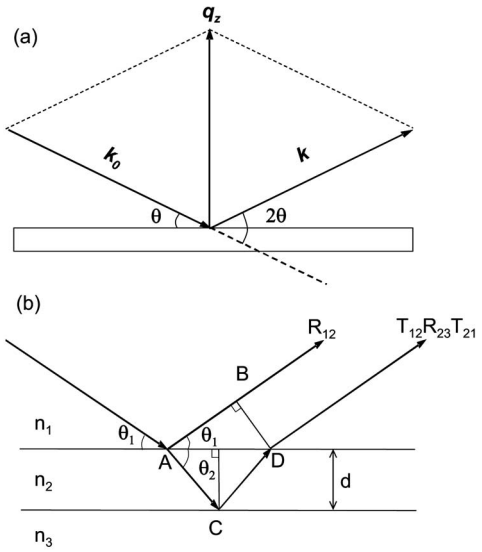

FIG. 1. Schematic of (a) scattering geometry and (b) bilayer interference. A recurring sequence of reflections occurs as each interface produces usually a transmitted beam and a reflected beam with $T_{ij}=1-R_i$. Similarly, multilayers produce a series of transmitted and reflected rays, the combined effect of which can be solved recursively (Ref. 12) The optical path length difference is equal to $n_2(\overline{AC}+\overline{CD})-n_1\overline{AB}$.

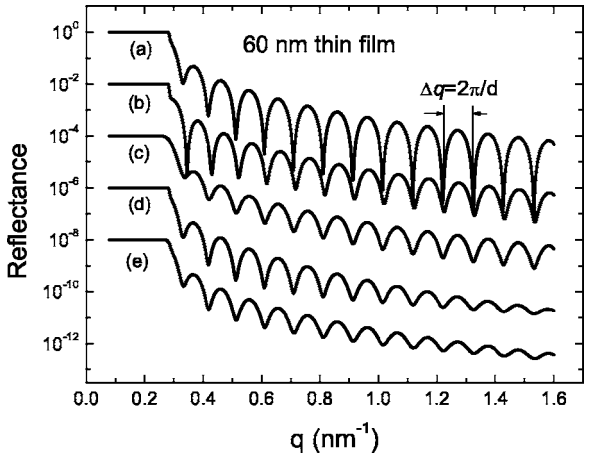

FIG. 2. Model reflectance profiles of 60 nm thin film of neutron reflectivity with $\lambda=0.475$ nm. (a) Perfect single layer with no roughness, matched reflected intensity from the top interface and bottom interface, i.e., $R_{12}=R_{23}$. (b) Same as (a); but reflectance from the bottom interface is $\frac{1}{4}$ of the intensity reflected from the top interface, i.e., $R_{23}=1/4R_{12}$. (c) Same as (a), but with $\Delta q_{\min}$ limitation due to beam angular divergence $\Delta\theta=1$ mrad. (d) Same as (a), but with surface roughness, $\sigma=1$ nm. (e) Same as (a), but with a wavelength spread $\Delta\lambda/\lambda=2.5\%$ ($\lambda=0.475$ nm).

trademark of conventional XR. In addition to the inherent or enhanced ability to distinguish materials, the utility of a particular reflectivity technique is strongly influenced by the intensity, wavelength, angular divergence, and longitudinal and transverse coherence properties of the probing beam as well as the angular resolution of the detector. Here, we will further detail the principles of RSoXR, delineate the capabilities, and provide a direct comparison to the well established techniques of conventional XR and NR.

Polystyrene (PS) and poly(methyl methacrylate) (PMMA) bilayers, one of the most intensively studied polymer bilayers, have been used as the primary demonstration sample. Several other bi- and multilayer polymer systems have also been studied as examples of the capabilities of RSoXR. Experiments and simulations show that RSoXR has a strong and controllable contrast near the carbon K edge and that polymer thin film properties can be characterized without the need for chemical modification. A direct comparison of RSoXR with XR and NR using two respective sets of identical samples is provided. RSoXR is shown to provide very accurate interfacial information, demonstrating that it is an excellent alternative tool to XR and NR with unique strengths for the study of polymer interfaces and organic thin films in general.

II. PRINCIPLES

Specular reflectivity techniques probe the profile of the film along the z direction by measuring the reflectance as a function of momentum transfer along the surface normal, q_z, in a so-called θ-2θ scan (see schematic in Fig. 1). Hence,

$$q_z=|k-k_0|=\frac{4\pi\sin\theta}{\lambda}, \tag{1}$$

where k_0 and k are the wave vectors of the incident and scattered beams, respectively, θ is the incident angle, and λ is the wavelength of the probe beam used [Eq. (1) is valid for both x rays and neutrons]. When studying thin films with reflectivity, one generally characterizes the interference of beams reflected at different interfaces. Due to constructive and destructive interference as a function of θ, and hence q_z, interference fringes are observed as a key feature of specular reflectivity. The intrinsic visibility of these interference fringes, in the absence of noise, depends on the matching of intensity of the interfering beams, which is directly related to the reflectance coefficient R_{ij} of the interface between layers i and j. The neutron reflectance of a model 60 nm thick single layer thin film with matched and mismatched reflectivities R_{12} and R_{23} at two interfaces are shown as an example in Figs. 2(a) and 2(b), respectively. In Fig. 2(a), the reflected intensity from the top interface R_{12} is the same as the reflected intensity from the bottom interface R_{23}. In Fig. 2(b), the reflectivity from the bottom interface is 1/4 of the intensity reflected from the top interface (i.e., $R_{23}=1/4R_{12}$), and this mismatch decreases the amplitude of the fringes. Sensitivity to distinguish materials depends thus on the ability to produce measurable and relatively well matched R_{ij}'s at the various interfaces. Reflectivity from multiple interfaces is similar and can be solved recursively.[12]

We note that the neutron, hard x-ray and soft x-ray communities use different languages to describe the interactions being observed. However, the underlying physics of these is essentially analogous. In the neutron community, the interaction with matter is described in terms of scattering length density, the hard x-ray community describes interactions in

terms of scattering factors and electron densities, and the soft *x* ray community describes interactions in terms of either scattering factors or index of refraction. Given that the wavelength of soft x rays is much larger than an atom, we have chosen to present the soft x-ray interaction from a solid state picture that utilizes the index of refraction. Hence, similar to optics with visible light, when a soft x-ray beam is reflected from the top of a sample, the reflectance coefficient R_{ij} for a perfect interface is given by the well known Fresnel formula

$$R_{ij} = r_{ij}^2 = \left| \frac{k_{zi} - k_{zj}}{k_{zi} + k_{zj}} \right|^2 = \left| \frac{n_i \sin \theta_i - n_j \sin \theta_j}{n_i \sin \theta_i + n_j \sin \theta_j} \right|^2, \quad (2)$$

where k_{zi} and k_{zj} are the perpendicular component of wave vectors in media i and j, and n_i, n_j are the respective indices of refraction (which include a dispersive δ and an absorptive β component, $n=1-\delta-i\beta$). θ_i is the incident angle and θ_j is the refraction angle in medium j (as shown in Fig. 1).

Equation (2) can most easily be extended by considering and utilizing Porod's law, which is being commonly utilized in small angel x-ray scattering and small angle neutron scattering. When describing this extension of Eq. (2) in terms of scattering length densities, the language used by the neutron community, one arrives at

$$R_{ij} \approx \frac{\pi^2 \{[\mathrm{Re}(\Delta\rho_s)]^2 + [\mathrm{Im}(\Delta\rho_s)]^2\}}{q^4}, \quad (3)$$

where $\Delta\rho_s$ is the difference in scattering length density between two media at an interface.[4] Equation (3) can be expressed in the solid state picture by exchanging the real and imaginary parts of $\Delta\rho_s$ for the corresponding index of refraction descriptions $\Delta\delta$ and $\Delta\beta$, and

$$R_{ij} \propto \frac{\Delta\delta^2 + \Delta\beta^2}{q^4}. \quad (4)$$

From Eq. (4) we can see that for any given q, the reflectivity is sensitive to differences in the index of refraction across an interface and is proportional to $\Delta\delta^2+\Delta\beta^2$. The term $\Delta\delta^2+\Delta\beta^2$ can therefore be considered a quantitative measure of the contrast between materials.

In real systems, the interfaces are either rough or diffuse, resulting in an effective composition profile at the interface.[13] Roughness and diffuseness affect the reflectance that will reduce the reflection coefficient r_{ij} by a roughness factor $\exp(-2k_{zi}k_{zj}\sigma_{ij}^2) \approx \exp(-q^2\sigma_{ij}^2/2)$, where σ_{ij} is the root mean square (rms) roughness of the interface, and k_{zi} and k_{zj} are the perpendicular component of the wave vectors in media i and j, respectively. So, the reflected beam intensity from a rough or diffuse interface decreases rapidly for rough interfaces. The q dependence of this roughness factor results in the damping of the reflectance fringes at large q [for an example see Fig. 2(d)].

The roughness of a sample is actually more complex than what can be accurately described by a single parameter such as σ_{ij}, with features spanning a range of length scales that often correspond to a unique spatial frequency Fourier spectrum. This Fourier spectrum can be composed of either a few dominant components that are usually the result of sample preparation conditions[14] or a large number of components as in the case of capillary waves. When measuring the roughness of a sample interface, the in-plane coherence length of the probe determines the longest spatial length scale, i.e., the lowest spatial frequency, that the experiment integrates over.[15–17] Hence, any measured rms roughness value will depend on the experimental conditions. A reconciliation between roughness values from reflectivity measurements and atomic force microscopy (AFM) measurements that exemplifies this issue has been discussed and provided by Yanagihara *et al.*[18] The in-plane coherence length is the projection of the transverse coherence properties of the beam onto the interfacial plane of interest, and thus does not only depend on the inherent beam properties but is coupled to the geometry of the experimental setup in the sagittal sample direction through the incident angle θ or q. For XR and NR, θ tends to be small, but for RSoXR in the soft x-ray range, θ is routinely $>20°$.

III. EXPERIMENT

The samples for RSoXR and XR were prepared on silicon (100) wafers (Wafer World), which were cleaved into 2.5 $\times$ 2.5 cm^2 substrates, and then were cleaned in Baker Clean JTB-111 (J.T. Baker) and washed with de-ionized (DI) water. They were then etched with 10% (v/v) hydrofluoric acid and rinsed with DI water to produce a hydrogen passivated silicon surface (Si–H). PMMA (Polymer Source, M_w = 154 kg/mol, M_w/M_n = 1.05, $T_g \approx 125$ °C) was spun from chlorobenzene (Sigma-Aldrich) on top of the substrates, annealed in vacuum at T = 150 °C for 8 h and quenched at room temperature through a simple removal from the oven. Subsequently, PS (Polymer Source, M_w = 138 kg/mol, M_w/M_n = 1.05, $T_g \approx 100$ °C) was spun from the selective solvent 1-chloropentane (Sigma-Aldrich) directly on top of the PMMA single layer.[14,19] Other polymer bilayer samples for RSoXR include PS/poly(2-vinyl pyridine) (P2VP) (Polymer Source, M_w = 100 kg/mol, M_w/M_n = 1.06, T_g = 100 °C) bilayer, poly(cyclohexyl methacrylate) (PCHMA) (Scientific Polymer Products, $M_w \sim 70$ kg/mol, T_g = 100 °C)/PMMA bilayer, poly(bromo-styrene) (PBrS)/PMMA bilayer, and PS/random polymer of styrene and acrylonitrile (SAN) M_w = 81.5 kg/mol, M_w/M_n = 1.09) bilayer, and were prepared using the same method. Samples for NR were prepared on silicon wafers 3 in. in diameter and 3 mm thick, with the dPS (Polymer Source, M_w = 139 kg/mol, M_w/M_n = 1.06, T_g = 100 °C) layer on top of the PMMA layer prepared using the same method used for the RSoXR samples. The bilayers were annealed in vacuum at 135 °C for 24 h and then quenched to room temperature. After quenching, the films were observed using visible light microscopy and AFM to assure that no dewetting has occurred.. Layer thicknesses were measured prior to and after bilayer formation with a Rudolph AutoEL-3 ellipsometer.

Near edge x-ray absorption fine structure (NEXAFS) spectra of reference samples were acquired at beamline 5.3.2 at the Advanced Light Source (ALS).[20] Reflectivity (θ–2θ) data sets were acquired at beamline 6.3.2 at the ALS in a

high vacuum ($\sim 10^{-7}$ torr).[21] The data acquisition time was about 10 min per angular scan ($\theta = 0° - 40°$). The angular resolution was ~0.3 mrad. The photon energy was calibrated by measuring absorption spectra of the samples at BL6.3.2 and by comparing to near edge resonance features of known spectra.[22,23] Using the 600 1/mm grating of that beamline, the resolving power is ~2000, and the beam intensity at the sample position is $\sim 10^{11}$ photons/s/0.1% BW. Given a typical beam size on the sample of 30×300 μm^2 at ~20°, this translate into a fluence of $\sim 10^{-9}$ J/m^2 at 285 eV. To detect and avoid radiation damage, which can cause mass loss and spectral change[24,25] and hence cause repeatability problems, some scans were repeated and the sample occasionally translated to expose a fresh sample area. Simulations and fits were performed using the noncommercial program IMD.[26] Conventional x-ray reflectivity data sets were acquired at Beamline X10B of the National Synchrotron Light Source (NSLS), Brookhaven National Laboratory, using a photon energy of 14.2 keV ($\lambda = 0.087$ nm). The total acquisition time was about 1 h, with the dwell time for each angle adjusted, depending on the scattering angle. The angular resolution $\Delta\theta = 0.02°/0.3$ mrad, and the wavelength spread $\Delta\lambda/\lambda$ was about 0.03%, so the instrument resolution Δq is ~0.04 nm^{-1}. Neutron reflectivity experiments were performed on the NG7 reflectometer at the NIST Center of Neutron Research (NCNR).[9] The incident cold neutron beam had a wavelength of 0.475 nm with a wavelength spread $\Delta\lambda/\lambda \sim 2.5\%$. The footprint of the beam on the sample and the instrument resolution $\Delta q/q$ were kept constant at ~0.04 by adjusting the slits between the monochromator and the sample. The data acquisition time was about 3 h for each sample.

IV. RESULTS AND DISCUSSION

A. RSoXR

Near absorption edges corresponding to soft x rays, the complex index of refraction, $n = 1 - \delta - i\beta$, of a polymer shows strong energy dependence due to the possibility to excite a bound electron within the material into bound or quasibound states. The bound states, in particular, can result in very sharp features that are intrinsically limited by the core-hole lifetime to about ~100 meV in width for carbon *K*-edge absorption. This strong energy dependence of β close to the edge is known as NEXAFS.[27] The same features, though less pronounced, can be found near absorption edges at higher energies (in the hard x-ray regime) but are instead known as x-ray absorption near edge structure (XANES).[28] Strong energy dependence is also observed for the index of refraction decrement, particularly for soft x rays. As examples of this strong energy dependence, Fig. 3 shows the index of refraction decrement δ and absorption index β for PS, PMMA, and P2VP in the vicinity of the carbon *K*-absorption edge. Here, β was obtained by acquiring a transmission NEXAFS spectrum from the respective polymer and by scaling the pre- and postedge to the Henke atomic scattering database,[29] taking into account the known

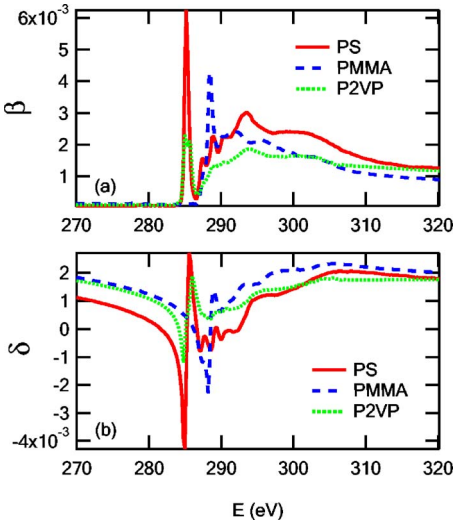

FIG. 3. (a) Absorption β and (b) index of refraction decrement δ of the complex index of refraction for PS, PMMA, and P2VP near the carbon *K* absorption edge. Both δ and β exhibit fine structure near the absorption edge that can be exploited to tune the reflectivity at an interface. (Note that these are improved calculation compared to those shown in Ref. 11).

composition of these materials. The index of refraction decrement δ was calculated from β through the Kramers-Kronig integral relations.[30] While in principle δ can be measured rather than calculated, the traditional interferometric measurements have not yet yielded extensive or accurate data sets near absorption edges in the soft x-ray region.[31] Presently, the calculations for δ via Kramers-Kronig relations from β, even when executed carefully, introduce some minor systematic errors.

It is clear in Fig. 3 that the complex index of refraction exhibits rapid changes near the absorption edge that depend strongly on the functional groups and molecular structure present in the polymers. The graphs for P2VP and their comparison to PS show how drastically δ and β can change if just a single carbon atom is replaced by a nitrogen heteroatom in an aromatic group. In general, the fine structure features in β and δ are more varied and pronounced in carbonaceous materials than in any other class of materials. The spectral richness of β is already used extensively in NEXAFS spectroscopy and soft x-ray microscopy of carbonaceous materials.[32,33] The NEXAFS absorption spectra of synthetic polymers compiled by Dhez[22] and Urquhart and Ade[23] and of biopolymers by Kaznacheyev *et al.*[34] can thus serve as a guide to how powerful and general resonant soft x-ray reflectivity will be beyond the specific systems utilized in the present demonstration.

Due to the low refraction of soft x rays, the reflectivity at any given angle (above the critical angle) scales approximately with $\Delta\delta^2 + \Delta\beta^2$, as demonstrated by Eq. (4). As a proxy metric on how strongly the reflectivity from the various interfaces can be controlled through the choice of photon energy, $\Delta\delta^2 + \Delta\beta^2$ is shown in Fig. 4(a) for the PS/PMMA, PS/vacuum, and PMMA/vacuum interfaces. In addition, the PS/P2VP, P2VP/vacuum, and P2VP/PMMA interfaces are shown in Fig. 4(b), and $\Delta\delta^2 + \Delta\beta^2$ is shown for PS/PMMA

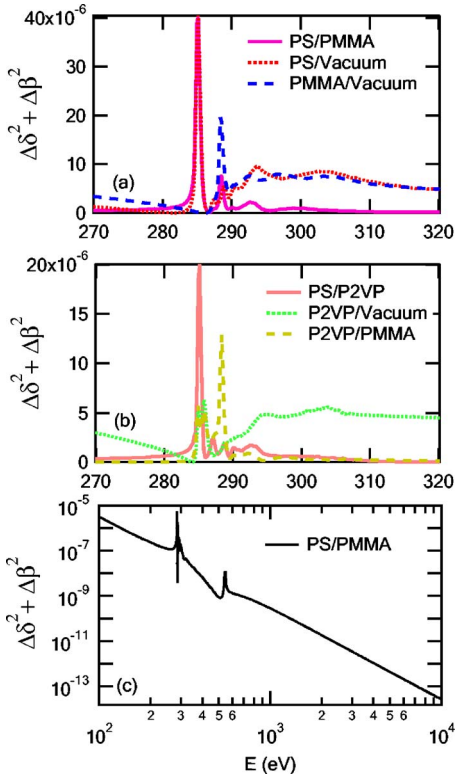

FIG. 4. (a) Relative reflectivity of PS/PMMA, PS/vacuum, and PMMA/vacuum interfaces near the carbon *K* edge. (b) Relative reflectivity of PS/P2VP, P2VP/vacuum, and P2VP/PMMA interfaces. (c) Reflectivity of the PS/PMMA interface for a larger range of photon energies. The feature near the oxygen edge at ~540 eV does not take into account the finer details that one would expect for PMMA, but is solely due to the edge jump based on the absorption data tabulated by Henke *et al.* (Ref. 29).

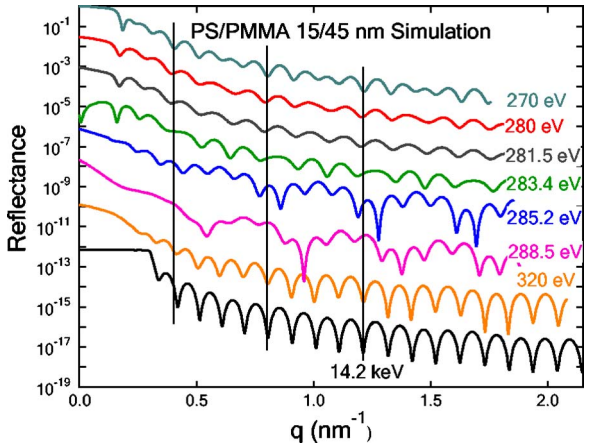

FIG. 5. Calculated reflectance of a perfectly smooth 15 nm/45 nm PS/PMMA bilayer at selected photon energies using the values of δ and β displayed in Fig. 3. At 14.2 keV and 320 eV, the fringes are dominated by the sensitivity to the total film thickness. In contrast, fringes at 280.0, 281.5, 283.4, 285.2, and 288.5 eV show a strong sensitivity to the polymer/polymer interface.

over a larger energy range in Fig. 4(c). As observed for δ and β, large and rapid changes of the reflectivity as a function of photon energy are apparent near absorption edges. These measures are important because, as shown in Fig. 2, matching of the reflectivity from different interfaces translates directly into fringe visibility.

We will first focus on PS/PMMA bilayers on Si–H substrates as a model system. As can be seen in Fig. 4, the reflectivity from the PS/PMMA interface is very strong at 285.2 and 288.5 eV, so high sensitivity to the PS/PMMA interface can be expected at these energies. At higher energies, the reflectivity at a PS/PMMA interface becomes small compared to the PS/vacuum interface, which makes it more difficult to observe the PS/PMMA interface. This relationship extends to the hard x-ray energies and is the reason why the ability to distinguish polymers is low at such high energies. An interesting energy to consider, based on calculated values of the index of refraction decrement δ, is at ~281.5 eV. At this energy $\delta=0$ and β is very small for PS. Hence, the x rays cannot significantly distinguish vacuum from PS, and the reflection from the PS-vacuum interface is nearly absent. A PS layer on top will become essentially invisible at this energy and only the bottom PMMA layer will be observed.

The complex photon energy dependence of the index of refraction for polymer bilayers is best illustrated by simulations, as they provide perfect control of the involved parameters. As discussed above, the intensity of the reflected beam at individual interfaces is strongly energy dependent. A similar strong energy dependence is expected for the reflectance from PS/PMMA bilayers supported on Si–H substrates, considering that it is the result of interference between the three energy dependent reflections at each interface. Simulations of a sample of a 15 nm PS on top of 45 nm PMMA on silicon, where the thickness ratio is 1:3, show the most salient aspects quite clearly (Fig. 5). For maximum clarity, the surface and interface roughnesses are set to zero. For 320.0 eV and 14.2 keV photon energies, almost uniform modulations, referred to here as interference fringes and often called Kiessig fringes, with $\Delta q \approx 0.105$ nm^{-1} and hence $d \approx 2\pi/\Delta q = 60$ nm are observed. These fringes thus arise from the interference of reflected beams from the PS/vacuum and PMMA/Si interfaces and show very limited sensitivity to the polymer-polymer interface. In contrast, strong interference effects related to the bilayer structure are readily observed as beats (i.e., modulations of the fringe amplitude) at photon energies of 285.2 and 288.5 eV. The simulation at 285.2 eV has, for example, strong beats corresponding to $\Delta q \approx 0.42$ nm^{-1}, which is four times the Δq that corresponds to the full thickness. This directly implies strong sensitivity to the 15 nm thick PS layer, which is 1/4 of the total film thickness. At 270.0 eV, good sensitivity to the PS/PMMA interface is observed, although the overall fringe amplitude is reduced compared to 285.2 eV, due to the increased mismatch of the relative reflectivities as discussed in the Introduction. At 281.5 eV, we observe uniform fringes with the fringe spacing $\Delta q \approx 0.14$ nm^{-1}. These correspond to a film thickness of ~45 nm, which is 4/3 of the fringe spacing observed at 320 and 14.2 keV. This shows that at 281.5 eV, only the 45 nm PMMA would be observed when the index of

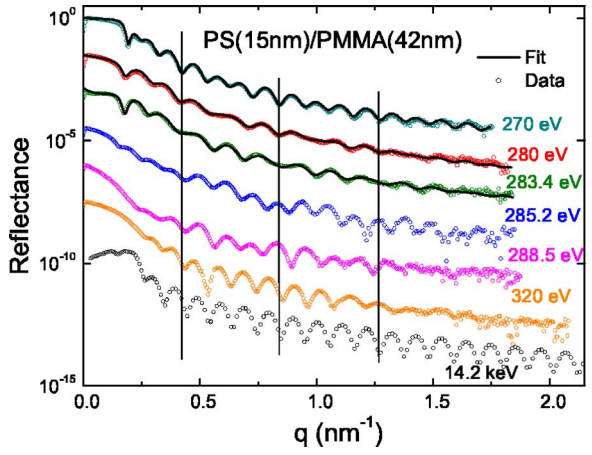

FIG. 6. Experimental data (circle) of a 15 nm/42 nm PS/PMMA bilayer acquired at 270, 280, 283.4, 285.2, 288.5, 320, and 14.2 keV (recorded at X10B, NSLS) and fits (solid line) for 270, 280, and 283.4 eV.

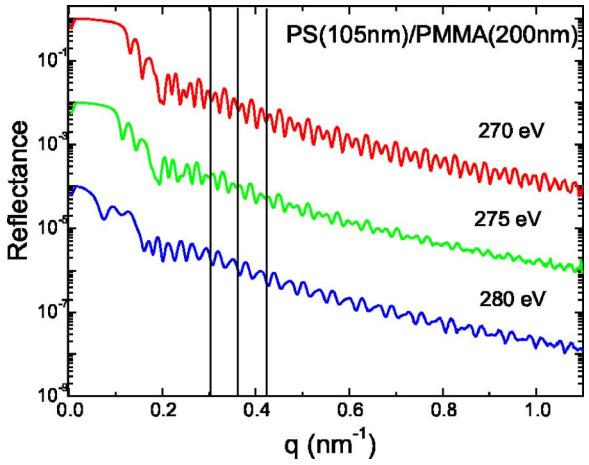

FIG. 7. Reflectance of a 105 nm/200 nm PS/PMMA bilayer acquired at 270, 275, and 280 eV.

refraction of the top layer PS ($\delta=0$, $\beta\approx 0$) is very close to the index of refraction of the vacuum ($\delta=0$, $\beta=0$) (Fig. 1). The PS is almost invisible at this energy, and the reflectivity fringes reflect only the information about the PMMA layer. At 280.0 and 283.4 eV, fringes similar to those for 281.5 eV can be observed. The slightly less uniform fringes indicate that there is still some sensitivity to the PS/vacuum interface at 280.0 and 283.4 eV. These simulations demonstrate that a careful choice of specific photon energies can greatly improve the sensitivity of resonant reflectivity to a specific interface relative to conventional XR. By using the energy where the reflection from the top layer can be selectively suppressed, we will be able to obtain information just about the polymer interface when the effect of the substrate interface is well known.

Figure 6 shows experimental data for a 15 nm/42 nm PS/PMMA bilayer for nominally the same soft x-ray photon energies used in the simulations shown in Fig. 5. Overall, the experimental data are in close agreement with the simulations, displaying the same strong photon energy dependence. At ~14.2 keV, where sensitivity to the polymer/polymer interface is very low, only fringes corresponding to the total layer thickness are observed. A strong beat effect in the reflectance fringes at 270.0, 283.4, 285.2, and 288.5 eV clearly shows the predicted sensitivity to the polymer-polymer interface. Vertical markers in the figure delineate two sets of four fringes with $\Delta q\approx 0.11$ nm^{-1}, which corresponds to $d=57$ nm, i.e., the total film thickness. At 280.0 and 283.4 eV, the experimental data show a weak beat frequency at this energy as the amplitudes of the fringes clearly change, with every fourth fringe almost completely suppressed, which gives the appearance as if only three fringes between the vertical markers are present. The average fringe spacing $\Delta q\approx 0.15$ nm^{-1} corresponds to the PMMA layer thickness $d=42$ nm. This agrees with the simulation that indicated that the PS layer should be nearly invisible at these energies. Interestingly, the 270.0 and 280.0 eV maxima and minima line up near the markers, whereas the 283.4 and 285.2 eV maxima and minima line up in-between markers. Inspection of the very low q range also shows that the critical angle gets smaller from 270.0 to 280.0 eV (as evidenced by a sharp drop in reflectivity at $q\approx 0.2$ nm^{-1}) and disappears entirely for 283.4 eV due to $\delta<0$ at that energy. This clearly indicates that δ has a zero crossing at an energy between 280.0 and 283.4 eV, with a corresponding phase shift of π as the x-ray beam reflects off the optically denser material at energies above the zero crossing ($\delta<0$) and without a phase shift when the x-ray beam reflects off the optically less dense material below the zero crossing energy ($\delta>0$). Only in the latter case is a critical angle observed. This is in good agreement with the derived δ plotted in Fig. 3, in which δ has a zero crossing at energy ~281.5 eV. More precise measurements (data not shown here) reveal that δ is 0 at 281.2 eV.

With strong and tunable sensitivity to both the PS/vacuum and PS/PMMA interfaces, RSoXR can simultaneously measure surface and interface roughness with high precision. Figure 7 shows the experimental data for a 105 nm/200 nm PS/PMMA bilayer at x-ray energies of 270.0, 275.0, and 280.0 eV. As previously seen for the thinner films, strong energy dependence can be observed in the reflectance.. The dominant fringe spacing Δq for the 280.0 eV data is 3/2 of that at other energies, indicating that this energy is more sensitive to the PMMA layer, which has a thickness ~2/3 of the total thickness. More importantly, even in the raw data at 270.0 eV, it is apparent that with increasing q the beating dies out more rapidly than the fringes that correspond to the total film thickness. This directly reflects the fact that the surface roughness is smaller than the interfacial width/roughness. Hence, fitting the profiles and extracting surface σ_s and interface σ_i, width/roughness values will be highly accurate without the need to keep the surface roughness a fixed parameter during fitting, or to provide it from an independent measurement. Note that the total film thickness used is ~300 nm, which is relatively thick compared to the thickness that conventional XR can typically probe.

The very high sensitivity of RSoXR to both interfaces is well illustrated in Fig. 8, showing 275 eV reflectivity data

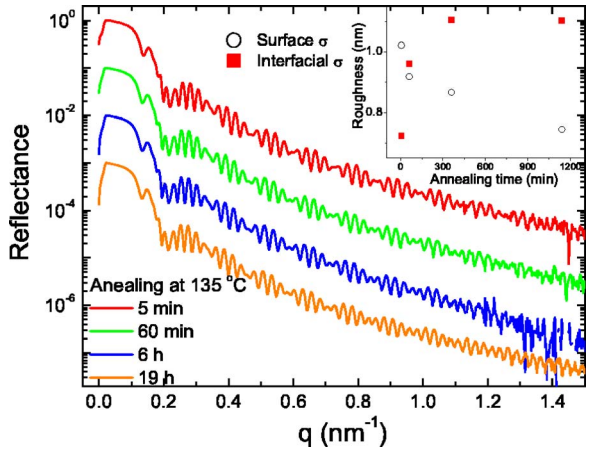

FIG. 8. Reflectance measured at 275 eV, for 50 nm/200 nm PS/PMMA bilayers annealed at 135 °C for 5 min, 60 min, 6 h, and 19 h (from top to bottom). The values of the surface roughness (open circle) and interfacial roughness (square) extracted from fits are plotted in the inset.

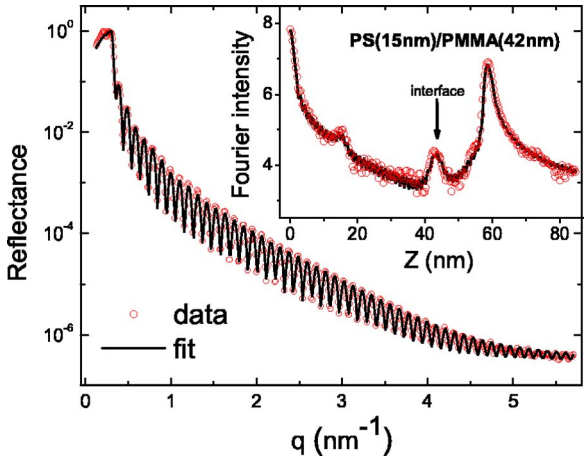

FIG. 9. Hard x-ray reflectance for a 15 nm/42 nm PS/PMMA bilayer acquired at 14.2 keV (recorded at X10B, NSLS—circle) and fit (solid line). The inset shows a Fourier analysis of the data. Note that the measured q range reaches nearly 6 nm^{-1} due to the high energy of the x-ray beam.

from four nominally identical 50 nm/200 nm PS/PMMA bilayers that have been annealed at 135 °C for 5 min, 1 h, 6 h, and 19 h. While fitted values of the surface and interfacial roughness are plotted against annealing time in the inset of Fig. 8, the evolution of the surface and interface can be qualitatively observed directly from the plotted raw data. For the bilayer annealed for 5 min, only the residual solvent is removed, leaving the surface still very rough from the spin casting. In contrast, the interface is initially very smooth, with only ~0.7 nm roughness, leading to strong beating that persists to the highest q values. With longer annealing times, the surface becomes smoother and the polymers interdiffuse at their interface (approaching their thermodynamic equilibrium), leading to an increase in the measured interfacial width/roughness. After 6 h of annealing, the interface reaches equilibrium at ~1.1 nm roughness, a value very similar to that measured after 19 h of annealing. In contrast, the surface requires longer annealing to reach equilibrium. After 19 h the surface roughness is ~0.7 nm, which is very close to previously reported values.[10,35,36] This situation seems somewhat counterintuitive, as the surface, having the higher interfacial tension and higher mobility, should more quickly come to equilibrium. While such reasoning is correct for the local concentration and small wavelength roughness, the top film likely has a dominant ~10–30 μm scale roughness component (originating from the process of spin casting directly from 1-chloropentane) that takes longer to anneal out.[14]

B. Comparison of RSoXR to XR and NR

A direct comparison of RSoXR to XR and NR was made using two sets of samples. For the comparison between RSoXR and conventional XR using the Fourier analysis developed by Seeck *et al.*, the thinner 15 nm/42 nm PS/PMMA bilayers were utilized due to the thickness limitation of XR. The very same bilayer sample was characterized using both techniques. The XR data and analysis are plotted in Fig. 9, while the RSoXR data and fit are plotted in Fig. 6. The results of RSoXR and XR are summarized and compared in Table I. From RSoXR, the interfacial roughness is determined to be ~1.2 nm, whereas XR yields ~1.0 nm. The surface roughness is ~0.8 nm for RSoXR and ~0.5 nm for Fourier analysis hard x-ray reflectivity. Results from both techniques agree reasonably well with each other. We note that the in-plane coherence length of RSoXR is about 80 μm, while that of XR is ~1 μm. Therefore, the range of Fourier roughness components included in the RSoXR measurement is larger than for XR. The difference in the in-plane

TABLE I. Result of RSoXR and Fourier analysis XR of the 15 nm/42 nm PS/PMMA bilayer.

Method	E (eV)/λ (nm)	D (nm) PS	D (nm) PMMA	σ_{rms} (nm) PS/air	σ_{rms} (nm) PS/PMMA
RSoXR	270/4.59	15.5	42.2	0.82	1.12
	280/4.42	15.9	42.0	0.79	1.22
	283/4.38	15.6	42.2	0.80	1.15
	Average	15.7	42.1	0.80	1.16
Fourier analysis XR	14.2 K/0.087	15.5	42.6	0.45	0.99

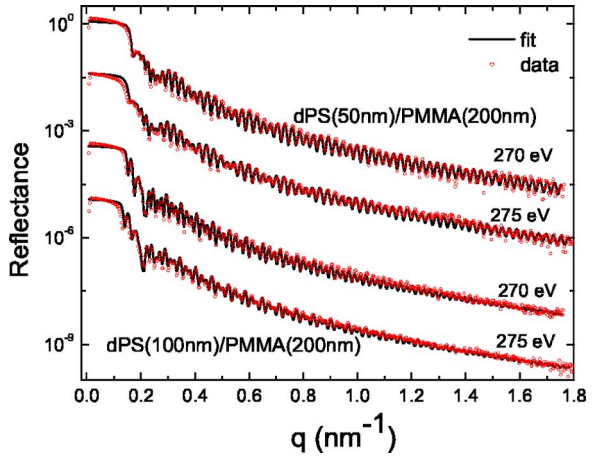

FIG. 10. Soft x-ray reflectance of 50 nm/200 nm and 100 nm/200 nm dPS/PMMA bilayers at 270 and 275 eV. Circles represent measured RSoXR data, while solid lines are fits.

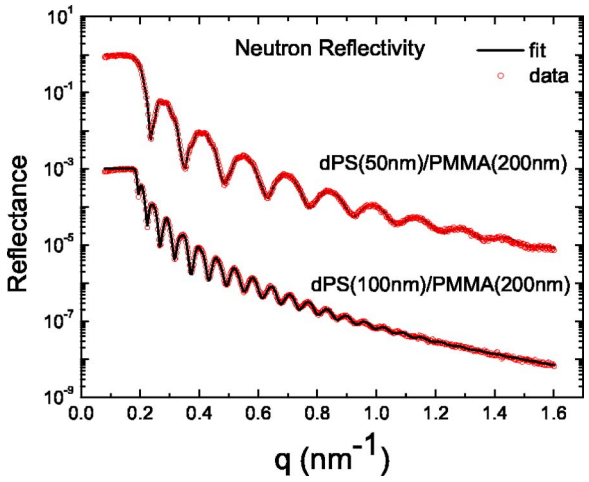

FIG. 11. Neutron reflectance for dPS (50 nm)/PMMA (200 nm) bilayer and dPS (100 nm)/PMMA (200 nm) bilayer. Circles represent measured NR data, while solid lines are fits.

coherence length (see below) thus results in a roughness value measured by RSoXR that is larger than the XR measured roughness value.

A comparison of RSoXR to NR required characterizing bilayers with one deuterated species on relatively large substrates. Deuterated PS (dPS) was utilized. dPS/PMMA bilayers of 50 nm/200 nm and 100 nm/200 nm in thickness were studied. These samples were first analyzed at the NG7 reflectometer, NCNR, NIST, and subsequently with RSoXR at beamline 6.3.2 at the ALS. Data and fits of RSoXR are plotted in Fig. 10. Fitting of the 270.0 eV data was somewhat easier and converged more readily than the 275 eV due to the higher relative accuracy of the index of refraction at 270.0 eV. However, minor inaccuracies in the index of refraction do not affect the final result of the interfacial values. The NR data and fits are shown in Fig. 11. During the fitting of the NR data, slight changes in the resolving power, $\Delta\lambda/\lambda$, were observed to greatly affect the fitted interfacial roughness value without significant change in the quality of the fit. This was especially the case for the films with the 100 nm PS on top, for which significantly greater interfacial roughness values were obtained if the resolving power parameter was fixed at a slightly smaller value. The film thickness is clearly in the range dictated by the instrument resolution as discussed in the following section. Hence, it is important to know the spectral purity of the beam accurately to analyze the data with confidence. Results for best effort fits for both RSoXR and NR are summarized in Table II. The interfacial roughness determined by RSoXR is ~1.5 and ~1.4 nm by NR. The surface roughness is ~0.6 nm for RSoXR and ~0.4 nm for NR. A very good agreement between both techniques was obtained. This verifies the sensitivity and accuracy that can be achieved with RSoXR. Because of the larger in-plane coherence length of RSoXR compared to NR, the measured roughness values are expected to be slightly larger for RSoXR. On account of the intrinsic instrument resolution for RSoXR and NR and the particular film thickness utilized, the RSoXR values should be more accurate.

C. Comparison of techniques in terms of instrument parameters

While the different probe beams utilized by the different reflectivity variants result in obvious differences in material contrast, the practicality and utility of each depend heavily on the implementation of the experiment, which is best described in terms of instrument parameters. These parameters include the wavelength, the wavelength spread or resolving power, the longitudinal and transverse (lateral) coherence, the intensity, the divergence of the probing beam, the angular

TABLE II. Result of RSoXR and NR of 50 nm/200 nm and 100 nm/200 nm dPS/PMMA bilayers.

Method	Bilayers	D (nm) dPS	D (nm) PMMA	σ_{rms} (nm) dPS/Air	σ_{rms} (nm) dPS/PMMA
RSoXR	dPS (50 nm)/ PMMA (200 nm)	43.3	187	0.55	1.38
	dPS (100 nm)/ PMMA (200 nm)	98.5	189	0.77	1.48
Neutron reflectivity	dPS (50 nm)/ PMMA (200 nm)	41.7	189	0.43	1.34
	dPS (100 nm)/ PMMA (200 nm)	96.5	190	0.49	1.46

TABLE III. Comparison of NR, XR and RSoXR, as utilized in this work, in terms of instrument parameters.

	NR (NG7)	XR (X10B)	RSoXR (BL6.3.2)
λ	~0.5 nm	~0.1 nm	~4 nm
$\Delta\lambda/\lambda$	$\sim 10^{-2}$	$\sim 10^{-4}$	$\sim 5\times 10^{-4}$
$\xi_l=\lambda^2/2\Delta\lambda$	~25 nm	~500 nm	~4000 nm
ξ_t	20 μm	1 μm	80 μm
$\Delta\theta$	0.02°/0.3 mrad	–0.02°/0.3 mrad	0.02°/0.3 mrad
$\Delta q_{\min}$ at $q=2$ nm^{-1}	~0.028 nm^{-1}	~0.038 nm^{-1}	~0.0015 nm^{-1}
$d_{\max}\approx 2\pi/\Delta q_{\min}$	~230 nm	~170 nm	~4400 nm

resolution of the detector, and any background scattering or detector noise. We will discuss most of these parameters explicitly in the context of the presented data and specific experiments undertaken in this work. A summary of the calculated instrument parameter values is presented in Table III.

Since reflectivity observations are geometrically limited to $\theta_{\max}\leqslant 90°$, it can be seen from Eq. (1) that the wavelength of the probe beam directly affects the range of q that can be reached. For XR and NR, the wavelength λ is usually several angstroms and the theoretical q range can be very large. In practice however, the intensity falls off by $\sim q^4$ for perfect interfaces and even steeper for rough interfaces. Hence, the finite intensity of the source and possibly the dynamic range of the detector limit the q range by data acquisition times that produce acceptable S/N ratios at high q. For RSoXR near the carbon K edge, the wavelength is ~4 nm and the q range is limited to a hard maximum (normal incidence) of $q_{\max}$ ~3 nm^{-1}, which is comparable to the practical q range of NR. In Fig. 9 it is evident that XR can reach a much higher q range, which allows probing of smaller length scales and can increase precision. Since most soft x-ray beamlines have the carbon K edge at the bottom end of their capable spectrum, the q range of RSoXR can be significantly extended by performing additional measurements at higher soft x-ray energies. Furthermore, measurements near the nitrogen and oxygen K edges would extend the q range while possibly retaining the molecular structure derived contrast of RSoXR.

In reflectivity, information about the thin film is encoded in the interference between the reflected beam from different interfaces. Interference between the top and bottom interfaces can only be observed when the optical path difference between rays reflecting from different interfaces is not larger than the longitudinal coherence length ξ_l of the beam, i.e., $2d\sin\theta\leqslant\xi_l$, where d is the layer thickness (see Fig. 1). The longitudinal coherence length ξ_l is directly related to the spectral purity (i.e., resolving power $\lambda/\Delta\lambda$) of the beam as $\xi_l=\lambda^2/2\Delta\lambda$. Hence, the maximum thickness $d_{\max}$ of a film that can be probed is limited to $d_{\max}<(\lambda^2/2\Delta\lambda)/(2\sin\theta_{\max})$, where $\theta_{\max}$ is the maximum incident angle used in the measurement. A different kind of film thickness limitation is imposed by the angular beam spread; i.e., its divergence $\Delta\theta_b$ and detector resolution $\Delta\theta_d$ translate into a minimum $\Delta q_{\min}$. These limitations in angular resolution and the need for interferences can be combined and are referred to as instrument resolution,[7] with

$$\Delta q_{\min}=\frac{4\pi(\cos\theta)\Delta\theta}{\lambda}+q\frac{\Delta\lambda}{\lambda}=\sqrt{\left(\frac{4\pi}{\lambda}\right)^2-q^2}\Delta\theta+q\frac{\Delta\lambda}{\lambda}, \tag{5}$$

where $\Delta\theta=(\Delta\theta_b^2+\Delta\theta_d^2)^{1/2}$. The first term on the right side of Eq. (5) arises from the limited angular resolution, and the second term from the spectral resolution. For hard x rays and neutron, due to their short wavelengths, relatively small scattering angles will cover a sufficiently large q range. This, in turn, requires high angular resolution (i.e., small $\Delta\theta$) to achieve a good instrumental resolution (i.e., small $\Delta q_{\min}$).

We note that if one considers the errors in angles (divergence and detector resolution) and in wavelength in Eq. (1), then the error propagation rules would result in a $\Delta q_{\min}$ similar to Eq. (5), except that the terms are added in quadrature rather than linearly. This would result in a $\Delta q_{\min}$ that is a factor of $\sqrt{2}$ smaller than Eq. (5) for the case in which angular and wavelength limitations make matched contributions.

The q dependence of the two terms in Eq. (5) is complementary and emphasizes the angular limitation at low q and the wavelength resolving power at high q, respectively. If the instrument resolution is dominated by the second term of Eq. (5), it will result in damping of the fringes at higher q that resembles the damping caused by roughness at the interface [Figs. 2(d) and 2(e)].[37,38] Differentiation between the two effects can be difficult in practice, and so when attempting to characterize samples known to have a high interfacial width/roughness, it is advised to utilize thinner samples for which the effects of spectral resolution are reduced. Dominance of the instrument resolution by the angular term results in reduced visibility of fringes at low q, which cannot, however, be confused with roughness.

For typical neutron reflectometers, such as NG7 at NIST, the angular resolution is ~0.02°/0.3 mrad and with wavelength resolving power $\Delta\lambda/\lambda=1\%$ at $\lambda\sim 0.5$ nm; for a given q of 2 nm^{-1}, the first term in Eq. (5) is ~0.0075 nm^{-1} and the second term is 0.02 nm^{-1}. This gives a $\Delta q_{\min}$ of ~0.0275 nm^{-1}, which corresponds to a maximum thickness of ~230 nm that can be probed. For conventional hard x-ray XR, similar to NR, the angular resolution is ~0.02°/0.3 mrad and with wavelength resolving power $\Delta\lambda/\lambda=0.01\%$ at $\lambda\sim 0.1$ nm; for a given q of 2 nm^{-1}, the first term in Eq. (5) is ~0.0377 nm^{-1} and the second term is 0.0002 nm^{-1}. This gives a $\Delta q_{\min}$ of ~0.0379 nm^{-1}, which corresponds to a maximum thickness of ~170 nm. We can see that the instrument resolution of conventional XR is primarily limited by the angular resolution. For RSoXR, with similar instrument angular resolution to NR and XR, $\Delta\theta$ is ~0.02° (~0.3 mrad) and the wavelength spread $\Delta\lambda/\lambda=0.05\%$ at $\lambda\sim 4$ nm. For a given q of 2 nm^{-1}, the first term in Eq. (5) is ~0.0004 nm^{-1} and the second term is 0.001 nm^{-1}. This gives a $\Delta q_{\min}$ of ~0.0015nm^{-1}, which corresponds to a maximum probable thickness of ~4400 nm (will not be limited by absorption when using photon energies below the absorption edge). Clearly, RSoXR can achieve a very high instrument resolution that will allow the characterization of relatively thick films. The spectral purity

of the neutron beam at the new spallation neutron source, using a time of flight (TOF) method, will be increased to ~0.1%, thus greatly improving the capability of NR to analyze thicker films.[39]

The transverse coherence length (lateral coherence length), ξ_t, determines, along with the beam profile and experimental geometry, the distance between two points on the sample from which scattered rays will interfere coherently at the detector, i.e., the in-plane coherence length. The measured roughness values at an interface is the integration over a range of spatial frequency components, and the in-plane coherence length will set a limit on the longest spatial length probed. Hence, the measured roughness will depend on the transverse coherence length and the instrumental geometry.[40] For the instruments used in this work, we derived the following coherence lengths: XR at X10B, NSLS, had a transverse coherence length ξ_t of ~1 μm; NR at NG7, NIST, had a transverse coherence length of ~20 μm; and RSoXR at ALS BL6.3.2 had a transverse coherence length of ~80 μm. Due to the various degrees by which the in-plane coherence length changes during the data acquisition on account of the sample rotation and possible slit width changes, a rigorous, direct and quantitative comparison of this parameter between the different tools is presently not possible. However, for many studies these systematic differences are not very important since it is often the differences measured between a set of samples analyzed with the same instrument that is most relevant.

Acquisition times for NR, XR, and RSoXR were ~3 h, ~2 h, and ~10 min, respectively. Although no rigorous comparison assuring the same S/N has been made, there appears to be an advantage of RSoXR in terms of the time spent gathering data. Another practical consideration is the required sample size. For NR, samples must be at least 5 cm in diameter, whereas for XR and RSoXR, 1 cm diameter samples are more than sufficient—significantly relaxing sample preparation requirements.

Another issue requiring consideration is radiation damage. Neutron experiments do not result in damage to the sample. Hard x rays typically do not damage the polymer film directly, but via the secondary electrons created in the substrate. Working at low x-ray energies near the carbon K edge, one must be mindful that the absorption of x rays in the thin film itself can cause radiation damage of the organic materials. Absorption is very high at photon energies above the threshold, which would thus be an energy range typically avoided. The overall damage effects for the characterization of thin polymer films have been analyzed by Richter *et al.*[41] The relative radiation sensitivity has been delineated by Coffey *et al.*[25] Fortunately, there is a strong contrast for most polymer pairs below the absorption edge where the absorption is low. Furthermore, radiation damage can be mitigated by frequently changing the exposed sample area if the beam is very small or by increasing the beam size to reduce the average radiation per unit area. RSoXR is still in its infancy, and the best experimental protocols have yet to be developed.

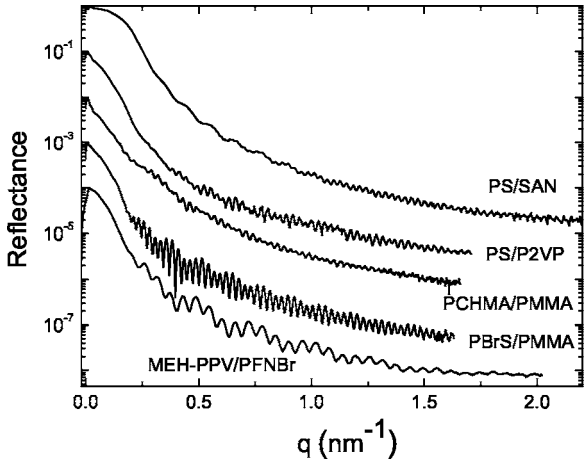

FIG. 12. RSoXR reflectance for a variety of polymer bilayers. From top to bottom: 50 nm/200 nm PS/SAN bilayer acquired at 400.0 eV; 50 nm/200 nm PS/P2VP bilayer acquired at 287.0 eV; 50nm/200 nm PCHMA/PMMA bilayer acquired at 286.1 eV; 50 nm/200 nm PBrS/PMMA bilayer acquired at 281.2 eV; 20 nm/80 nm MEH-PPV/PFNBr bilayer acquired at 285.1 eV.

D. Bilayers other than PS/PMMA and PS-*b*-PMMA multilayers

As shown above, an analysis of PS/PMMA bilayers using RSoXR yields very informative results. To further exemplify the capability of RSoXR, an analysis has been extended to a number of other bi- or multilayer polymer systems. Figure 12 displays the reflectivity data acquired at selected photon energies of the following polymer bilayers: (i) a nominal 50 nm/200 nm PS/P2VP bilayer (acquired at 287.0 eV), (ii) a nominal 50 nm/200 nm PCHMA/PMMA bilayer (acquired at 286.1 eV), (iii) a nominal 50 nm/200 nm PBrS/PMMA bilayer (acquired at 281.2 eV), (iv) a nominal 80 nm/20 nm poly[2-methoxy-5-(2′-ethylhexyloxy)-*p*-phenylene vinylene] (MEH-PPV)/poly[9,9-bis(6′-*N*,*N*,*N*,-trimethylammoniumhexyl)fluorene-co-alt-1,4 phenylene bromide] (PFNBr) bilayer (acquired at 285.1 eV),[42–45] and (v) a nominal 50 nm/200 nm PS/SAN bilayer (acquired at 400.0 eV, which is close to the nitrogen 1*s* edge). These polymer pairs have only small differences in electron density, resulting in relatively low contrast using conventional XR. In contrast, the RSoXR data from these bilayer systems show sufficient if not excellent sensitivity at good S/N to the polymer/polymer interface, as manifested by the clearly observable beats. The photon energy most sensitive to the polymer/polymer interface has not yet been determined for many of these bilayer systems. It requires improved knowledge about the complex index of refraction for these materials or a systematic change in photon energy.

Finally, we look at multilayered structures. Diblock polymer PS-*b*-PMMA thin films were studied as a model system. Approximately 200 nm thick films were prepared and annealed for times long enough to form a well defined lamellar structure. Reflectivity data acquired at 270.0, 275.0, and 280.0 eV are shown in Fig. 13. Bragg peaks, the signature of the multilayer structure, can be readily observed at all three

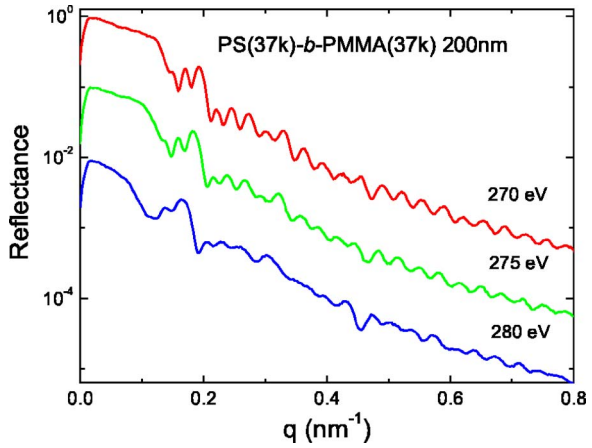

FIG. 13. RSoXR reflectance of a 200 nm thick lamellar PS(37*k*)-*b*-PMMA(37*k*) film acquired at 270 eV (top), 275 eV (middle), and 280 eV (bottom).

energies. The figure clearly demonstrates that information about multiple interfaces is present in these data.

E. Initial scientific results and future perspective

An interesting scientific application and initial result to date is the fact that the PS/PMMA bilayer has a measured interfacial roughness of 1.16 nm and is thus smaller than the width of 1.48 nm for the dPS/PMMA bilayer, as shown in Tables I and II. This is unexpected based on previously reported bulk Flory-Huggins parameters χ for PS/PMMA and dPS/PMMA.[46] Since $\chi_{\mathrm{PS/PMMA}} < \chi_{\mathrm{dPS/PMMA}}$, mean-field theory asserts that the width of a PS/PMMA interface would be greater than that of a dPS/PMMA interface (width $\propto \chi^{-1/2}$).[47] However, Harton *et al.*[48,49] have recently reported the strong preferential segregation of dPS to a dPS:PS/PMMA interface. The RSoXR results are qualitatively consistent with the results of Harton *et al.* and confirm that the thermodynamic properties of PS/PMMA interfaces are substantially different from those of the bulk.

NR was previously used to study capillary waves at the PS/PMMA polymer/polymer interface.[35] However, studies of thick films have been limited due to the small longitudinal coherence length of NR. Since RSoXR can study films up to microns thick and has much larger in-plane coherence length, it can be used to study capillary waves at polymer interfaces with relaxed thickness requirements. In addition, deuteration is not required for RSoXR and thus will eliminate the possible uncertainty induced by the isotope effect in the PS/PMMA system.

There are several potential further applications of RSoXR. For one, accurate values of the optical constants near absorption edges might be extracted by fitting the reflectivity of a single layer sample with known thickness and roughness. The thickness and roughness of the single layer can be determined at an x-ray energy away from the edge where the complex index of refraction can be precisely calculated.

Secondly, the principles of RSoXR can also be extended to nonspecular reflectivity, i.e., diffuse scattering.[50–52] In a number of cases, the tunable sensitivity for selected interfaces using soft x rays will allow the direct observation of a buried polymer/polymer interface with minimal interference from the polymer/vacuum interface. For the PS/PMMA bilayer, for example, there is a strong reflection from the PS/PMMA interface at 281 eV, but almost no reflection from the PS/air interface. Hence, the diffuse scattering will be dominated by the structure function of the PS/PMMA interface. In contrast, at 320 eV, the reflectivity is very high for the surface, and the diffuse scattering will be dominated by the contribution from the surface. Resonant diffuse scattering should thus lead to the direct observation of polymer/polymer interfacial properties and phenomena such as capillary waves.

RSoXR will also be an ideal tool to characterize the polymer-polymer interfaces in multilayer polymer light emitting diodes produced by spin casting from alternative polar and nonpolymer solvent. MEH-PPV/PFNBr, as shown in Fig. 12, is an example. MEH-PPV is a neutral conjugated polymer spun cast from toluene (nonpolar solvent) and PFNBr is a charged conjugated polymer (conjugated polyelectrolyte) spun cast from methanol (polar solvent). The quality of the interface between the two layers most likely significantly affects the electro-optical performance of the device; yet little is known about the interfacial properties of these or related materials.[42–44]

Furthermore, soft x-ray absorption of linearly polarized photons is sensitive to the relative orientation of bonds (x-ray linear dichroism), a phenomenon already exploited in NEXAFS microscopy.[53,54] This gives RSoXR the potential for contrast between different bond orientations within a polymer film and the possibility of studying changes in molecular orientation between the bulk and surface regions of thin polymer films. However, such a contrast mechanism would result in a complex change in optical constants as a function of q for p polarization, and the modeling of such results would be more complicated. The potential and implication of bond orientation need to be studied further. In the present geometry, s polarization is used, and the optical constants do not change as a function of q, even though the value of the optical constants might be affected by orientation in the sample.

V. CONCLUSIONS

RSoXR has been demonstrated to provide highly accurate information about organic thin films and their interfaces. We have discussed and demonstrated the "molecular structure specific" contrast mechanism that is utilized in RSoXR to distinguish organic materials without the requirement for chemical modifications (unlike neutron reflectivity, which commonly utilizes deuteration). Furthermore, we have demonstrated how the careful choice of photon energy allows the RSoXR contrast to be tuned to provide enhanced sensitivity to specific interfaces, especially polymer/polymer interfaces with example bi- and multilayer samples constructed from a variety of different polymers. Furthermore, we have shown that interface roughness measurements by RSoXR include a

wider range of the Fourier roughness spectrum than roughness measurements by conventional XR due to an increased transverse coherence length. RSoXR measurements are also more reliable than NR since the material properties can be inadvertently altered during the deuteration process. Additionally, we find RSoXR to have a number of practical advantages over XR and NR, including shorter acquisition times, relaxed minimum sample size requirements, and the capability to characterize thicker films. Having evaluated and discussed the capabilities and limitations of RSoXR, NR, and XR, we find RSoXR to be an excellent alternative tool for the characterization of thin organic films.

ACKNOWLEDGMENTS

The authors are grateful for fruitful discussions with and help from Sushil Satija (NIST) and Eric Gullikson (CXRO). The conjugated polymer bilayer sample was provided by A. Hexemer, A. Garcia, T.-Q. Nguyen, G. Bazan, K. Sohn, and E. Kramer (UCSB). Work at NCSU is supported by the U. S. Department of Energy (DE-FG02-98ER45737). Data acquired at beamlines 5.3.2 and 6.3.2 at the ALS, which is supported by the Director of the Office of Science, Department of Energy under Contract No. DE-AC02-05CH11231.

[1]E. J. Kramer, Physica B **173**, 189 (1991).
[2]R.-J. Roe, *Methods of X-Ray and Neutron Scattering in Polymer Science* (Oxford University Press, New York, 2000).
[3]J. Genzer and R. J. Composto, Polymer **40**, 4223 (1999).
[4]X. L. Zhou and S. H. Chen, Phys. Rep. **257**, 223 (1995).
[5]D. G. Bucknall, Prog. Mater. Sci. **49**, 713 (2004).
[6]T. P. Russell, Physica B **221**, 267 (1996).
[7]S. H. Anastasiadis, T. P. Russell, S. K. Satija, and C. F. Majkrzak, J. Chem. Phys. **92**, 5677 (1990).
[8]T. P. Russell, A. Karim, A. Mansour, and G. P. Felcher, Macromolecules **21**, 1890 (1988).
[9]C. F. Majkrzak, Acta Phys. Pol. A **96**, 81 (1999).
[10]O. H. Seeck, I. D. Kaendler, M. Tolan, M. Shin, M. H. Rafailovich, J. Sokolov, and R. Kolb, Appl. Phys. Lett. **76**, 2713 (2000).
[11]C. Wang, T. Araki, and H. Ade, Appl. Phys. Lett. **87**, 214109 (2005).
[12]L. G. Parratt, Phys. Rev. **95**, 359 (1954).
[13]D. G. Stearns, J. Appl. Phys. **65**, 491 (1989).
[14]D. Ennis, H. Betz, and H. Ade, J. Polym. Sci., Part B: Polym. Phys. **44**, 3234 (2006).
[15]F. P. Buff, R. A. Lovett, and F. H. Stillinger, Jr., Phys. Rev. Lett. **15**, 621 (1965).
[16]A. N. Semenov, Macromolecules **27**, 2732 (1994).
[17]S. K. Sinha, E. B. Sirota, S. Garoff, H. B. Stanley, Phys. Rev. B **38**, 2297 (1988).
[18]M. Yanagihara, T. Sasaki, M. Furudate, and M. Yamamoto, Opt. Rev. **3**, 65 (1996).
[19]S. E. Harton, F. A. Stevie, R. J. Spontak, T. Koga, M. H. Rafailovich, J. C. Sokolov, and H. Ade, Polymer **46**, 10173 (2005).
[20]A. L. D. Kilcoyne, *et al.*, J. Synchrotron Radiat. **10**, 125 (2003).
[21]J. H. Underwood and E. M. Gullikson, J. Electron Spectrosc. Relat. Phenom. **92**, 265 (1998).
[22]O. Dhez, H. Ade, and S. Urquhart, J. Electron Spectrosc. Relat. Phenom. **128**, 85 (2003).
[23]S. G. Urquhart and H. Ade, J. Phys. Chem. B **106**, 8531 (2002).
[24]E. G. Rightor, *et al.*, J. Phys. Chem. B **101**, 1950 (1997).
[25]T. Coffey, S. G. Urquhart, and H. Ade, J. Electron Spectrosc. Relat. Phenom. **122**, 65 (2002).
[26]D. L. Windt, Comput. Phys. **12**, 360 (1998).
[27]J. Stöhr, NEXAFS Spectroscopy (Springer, New York, 1992).
[28]A. Bianconi, Appl. Surf. Sci. **6**, 392 (1980).
[29]B. L. Henke, E. M. Gullikson, and J. C. Davis, At. Data Nucl. Data Tables **54**, 181 (1993).
[30]D. Attwood, *Soft X-Rays and Extreme Ultraviolet Radiation, Principles and Applications* (Cambridge University Press, Cambridge, England, 2000), pp. 90–94.
[31]C. Chang, E. Anderson, P. Naulleau, E. Gullikson, K. Goldberg, and D. Attwood, Opt. Lett. **27**, 1028 (2002).
[32]H. Ade, A. P. Smith, H. Zhang, G. R. Zhuang, J. Kirz, E. Rightor, and A. Hitchcock, J. Electron Spectrosc. Relat. Phenom. **84**, 53 (1997).
[33]S. G. Urquhart, A. P. Hitchcock, A. P. Smith, H. W. Ade, W. Lidy, E. G. Rightor, and G. E. Mitchell, J. Electron Spectrosc. Relat. Phenom. **100**, 119 (1999).
[34]K. Kaznacheyev, A. Osanna, C. Jacobsen, O. Plashkevych, O. Vahtras, and H. Agren, J. Phys. Chem. A **106**, 3153 (2002).
[35]M. Sferrazza, C. Xiao, R. A. L. Jones, D. G. Bucknall, J. Webster, and J. Penfold, Phys. Rev. Lett. **78**, 3693 (1997).
[36]M. Stamm and D. W. Schubert, Annu. Rev. Mater. Sci. **25**, 295 (1995).
[37]S. K. Sinha, M. Tolan, and A. Gibaud, Phys. Rev. B **57**, 2740 (1998).
[38]M. Tolan and S. K. Sinha, Physica B **248**, 399 (1998).
[39]L. K. Mansur and J. R. Haines, J. Nucl. Mater. **356**, 1 (2006).
[40]V. A. Chernov, V. I. Kondratiev, N. V. Kovalenko, S. V. Mytnichenko, and K. V. Zolotarev, J. Appl. Phys. **92**, 7593 (2002).
[41]A. G. Richter, R. Guico, K. Shull, and J. Wang, Macromolecules **39**, 1545 (2006).
[42]W. L. Ma, P. K. Iyer, X. Gong, B. Liu, D. Moses, G. C. Bazan, and A. J. Heeger, Adv. Mater. (Weinheim, Ger.) **17**, 274 (2005).
[43]X. Gong, S. Wang, D. Moses, G. C. Bazan, and A. J. Heeger, Adv. Mater. (Weinheim, Ger.) **17**, 2053 (2005).
[44]R. Yang, H. Wu, Y. Cao, and G. C. Bazan, J. Am. Chem. Soc. **128**, 14422 (2006).
[45]These are similar to the bilayers described in Refs. 40 and 41. A more complete description and analysis of the data, synthesis, and sample construction is in C. Wang, H. Ade, A. Hexemer, A. Garcia, Q. Nguyen, G. Bazan, K. Sohn, and E. Kramer (unpublished).
[46]T. P. Russell, Macromolecules **26**, 5819 (1993).
[47]E. Helfand and Y. Tagami, J. Polym. Sci., Polym. Phys. Ed. **9**, 741 (1971).
[48]S. E. Harton, F. A. Stevie, Z. Zhu, and H. Ade, J. Phys. Chem. B **110**, 10602 (2006).
[49]S. E. Harton, F. A. Stevie, and H. Ade, Macromolecules **39**, 1639 (2006).
[50]Y. S. Seo, T. Koga, J. Sokolov, M. H. Rafailovich, M. Tolan, and S. Sinha, Phys. Rev. Lett. **94**, 157802 (2005).
[51]H. Kim, A. Ruhm, L. B. Lurio, J. K. Basu, J. Lal, D. Lumma, S. G. J. Mochrie and S. K. Sinha, Phys. Rev. Lett. **90**, 068302 (2003).
[52]M. K. Sanyal, S. K. Sinha, K. G. Huang, and B. M. Ocko, Phys. Rev. Lett. **66**, 628 (1991).
[53]H. Ade and B. Hsiao, Science **262**, 1427 (1993).
[54]A. P. Smith and H. Ade, Appl. Phys. Lett. **69**, 3833 (1996).